

See discussions, stats, and author profiles for this publication at: <https://www.researchgate.net/publication/221725378>

Modeling the Interaction between Integrin-Binding Peptide (RGD) and Rutile Surface: The Effect of Cation Mediation on Asp Adsorption

ARTICLE in LANGMUIR · FEBRUARY 2012

Impact Factor: 4.46 · DOI: 10.1021/la204329d · Source: PubMed

CITATIONS

12

READS

20

5 AUTHORS, INCLUDING:



Chunya Wu

Harbin Institute of Technology

12 PUBLICATIONS 101 CITATIONS

[SEE PROFILE](#)



Adam Arnold Skelton

University of KwaZulu-Natal

27 PUBLICATIONS 267 CITATIONS

[SEE PROFILE](#)



Lukas Vlcek

Oak Ridge National Laboratory

67 PUBLICATIONS 682 CITATIONS

[SEE PROFILE](#)



Peter T Cummings

Vanderbilt University

518 PUBLICATIONS 11,681 CITATIONS

[SEE PROFILE](#)

Modeling the Interaction between Integrin-Binding Peptide (RGD) and Rutile Surface: The Effect of Cation Mediation on Asp Adsorption

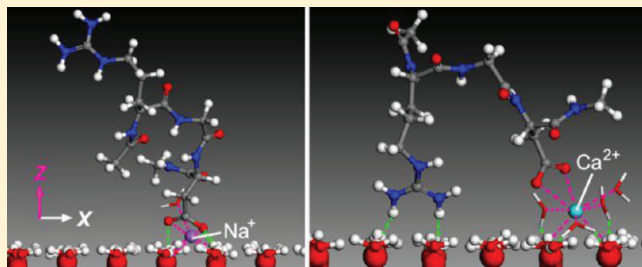
Chunya Wu,^{*,†,‡} Adam A. Skelton,^{‡,⊥} Mingjun Chen,[†] Lukas Vlček,[§] and Peter T. Cummings^{‡,||}

[†]Center for Precision Engineering, Harbin Institute of Technology, P.O. Box 413, Harbin 150001, China

[‡]Department of Chemical & Biomolecular Engineering, Vanderbilt University, Nashville, Tennessee 37235-1604, United States

[§]Chemical Sciences Division, ^{||}Center for Nanophase Materials Sciences, Oak Ridge National Laboratory, Oak Ridge, Tennessee 37831-6494, United States

ABSTRACT: The binding of a negatively charged residue, aspartic acid (Asp) in tripeptide arginine-glycine-aspartic acid, onto a negatively charged hydroxylated rutile (110) surface in aqueous solution, containing divalent (Mg^{2+} , Ca^{2+} , or Sr^{2+}) or monovalent (Na^+ , K^+ , or Rb^+) cations, was studied by molecular dynamics (MD) simulations. The results indicate that ionic radii and charges will significantly affect the hydration, adsorption geometry, and distance of cations from the rutile surface, thereby regulating the Asp/rutile binding mode. The adsorption strength of monovalent cations on the rutile surface in the order $Na^+ > K^+ > Rb^+$ shows a “reverse” lyotropic trend, while the divalent cations on the same surface exhibit a “regular” lyotropic behavior with decreasing crystallographic radii (the adsorption strength of divalent cations: $Sr^{2+} > Ca^{2+} > Mg^{2+}$). The Asp side chain in NaCl, KCl, and RbCl solutions remains stably H-bonded to the surface hydroxyls and the inner-sphere adsorbed compensating monovalent cations act as a bridge between the COO^- group and the rutile, helping to “trap” the negatively charged Asp side chain on the negatively charged surface. In contrast, the mediating divalent cations actively participate in linking the COO^- group to the rutile surface; thus the Asp side chain can remain stably on the rutile (110) surface, even if it is not involved in any hydrogen bonds with the surface hydroxyls. Inner- and outer-sphere geometries are all possible mediation modes for divalent cations in bridging the peptide to the rutile surface.



1. INTRODUCTION

The coating of bone-anchored implants aims at improved bone-implant contact and reduction of implant loosening and adverse reactions.¹ Over the past decade, considerable efforts have focused on the macro- and microporous coatings for bone ingrowth and bone-bonding ceramic coatings to promote early integration into the surrounding bone.^{2–7} However, to date, long-term clinical drawbacks still exist in terms of degradation and delamination of ceramic coatings. In addition, none of the coating technologies appear to act through biologically specific (e.g., receptor-mediated) mechanisms. The immobilization of biological factors onto an implant surface is a potentially more potent approach to induce a specific cellular response and promote long-term device integration.⁸ The arginine-glycine-aspartic acid (RGD) sequence, a ubiquitous adhesive motif in proteins, is regarded to be one of the best candidates for biomimetic coating of bone-anchored implants,^{1,8,9} due to three main reasons: i. RGD has a high affinity to $\alpha\beta_1$, the predominant osteoblast integrin;^{10,11} ii. Small peptides can be fabricated synthetically to high purity at relatively inexpensive cost and are independent of tertiary structure for bioactivity.⁸ iii. RGD coating on the implant surface (e.g., titanium implant⁸) is functionally stable in vitro.

The RGD precoating is expected to encourage cell adhesion⁹ and cell attachment¹² on the implant. However, a prerequisite

is that the precoated peptide layer must resist desorption caused by the competition with the soluble proteins in the serum solution¹³ and be subject to the combined effect of solvent (water, ions, etc.) and material characteristics (hydrophilicity, surface topography, surface charge, etc.). As addressed extensively in previous work, the water molecules arriving at the substrate surface earlier than the peptide have a profound influence on the peptide–surface interaction;^{14–16} furthermore, the surface properties determine the reactivity of the substrate in peptide/surface binding.^{17–21} Our previous simulation work found that the existence of Na^+ in the proximity of the negatively charged hydroxylated rutile (110) (surface charge density = -0.208 C/m^2 , pH ~ 7.80) significantly impacted aspartic acid (Asp) adsorption/arginine (Arg) desorption (residues in RGD).²² This motivated us to further elucidate the role of various cations in determining the binding propensity of RGD, especially the negatively charged residue (Asp), to the negatively charged rutile surface. Charge shielding by cations, which overcomes the electrostatic double-layer repulsion between the negatively charged adsorbate and the negatively charged adsorbent, has been confirmed in many

Received: November 4, 2011

Revised: January 3, 2012

Published: January 5, 2012



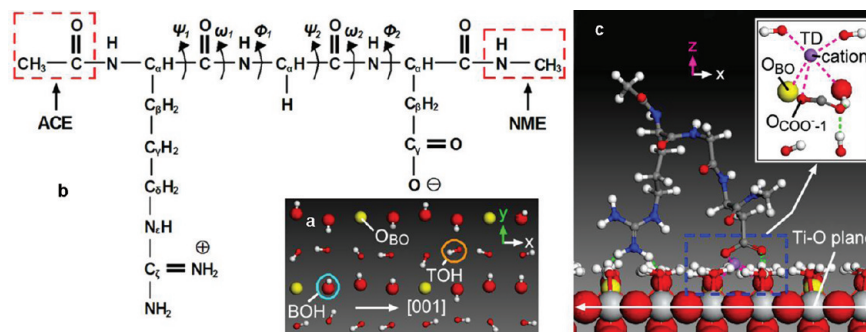


Figure 1. (a) Partial distribution of surface groups, (b) the structure of RGD tripeptide, and (c) the initial configuration of RGD on the negatively charged hydroxylated rutile (110) surface. The inset shows the COO⁻–surface binding site. The ACE and NME blocking groups are labeled by dashed rectangles.

experimental studies.^{23–27} Thomson et al.²³ pointed out that the surface charge of a mineral can be neutralized in the presence of sufficient Na⁺, making even negatively charged surfaces good adsorbents for the negatively charged adsorbates. Divalent cations, in particular Ca²⁺, were shown to be able to effectively neutralize negative surface charge of the mineral surface.^{24–26} Moreover, divalent cations were 100-fold more effective than monovalent cations in mediating the negatively charged DNA to the mineral surfaces.²⁷ Even though Na⁺ and K⁺ are typically much more abundant than Mg²⁺ and Ca²⁺ in body fluid, the latter may still be the principle mediators for protein adsorption on the implant surface. Therefore, the present work is intended to test the mediation mode and mediation stability of biologically important cations (Na⁺, K⁺, Mg²⁺, and Ca²⁺) and environmentally important cations (Rb⁺ and Sr²⁺) in Asp (of RGD)/rutile binding, where both of them are negatively charged, by means of MD simulations.

To further explore the tendency of cations toward surface or peptide binding, it is necessary to introduce the concept of “lyotropic effect”.^{28–30} A typical example of lyotropic effect is where anions and cations are arranged in the order of their adsorptivity from aqueous solutions on activated adsorbents. In the case of present study, this effect involves binding strength of cations to the negatively charged rutile surface as well as mediation of a peptide with the surface by a cation. A “regular” lyotropic effect when considering the binding characteristics of ions can be explained simply on the basis of hydration: ions of smaller crystallographic radii bind to the water molecules more strongly than those with larger radii. This causes the hydrated ion to be effectively larger with a more stable hydration shell, preventing as close an approach to the surface charged groups as that of an ion with less stable hydration shell, thereby resulting in a weaker electrostatic attraction.³¹ The “reverse” lyotropic effect is exhibited when ion–surface electrostatic attraction increases with decreasing crystallographic radii of the ions. Lyotropic sequences for simple ions at water–solid interfaces have been widely investigated,^{32–37} and it appears that the nature of the sequence (“regular” or “reverse”) depends on the nature of the surface.³⁸ The ‘regular’ lyotropic behavior of alkali cations was observed on the hydrophobic AgI and Hg surfaces, i.e., alkali cations of larger crystallographic radii showed greater tendency toward surface binding of AgI and Hg,^{32,33} however, for TiO₂ (anatase and rutile),³⁴ hematite (α -Fe₂O₃)^{35,36} and gibbsite (γ -Al₂O₃),³⁷ the adsorption affinity of alkali cations on the surface followed the ‘reverse’ sequence. Thus it is important to elucidate the lyotropic sequences for monovalent (Na⁺, K⁺, and Rb⁺) and divalent (Mg²⁺, Ca²⁺, and

Sr²⁺) cations at water-rutile interface at a molecular level; understanding the influence of the lyotropic behavior on cation mediation in Asp/rutile binding.

2. MATERIALS AND METHODS

2.1. Simulation Methodology. The isoelectric point (pI) of rutile is about 5.30 at 35 °C;³⁹ thus the negatively charged surface was considered in our simulations. The fully hydroxylated rutile surface was developed on the basis of the dissociative adsorption of water on the neutral nonhydroxylated surface. It is assumed that the hydroxyl from a water molecule binds to a 5-fold coordinated surface titanium and becomes a terminal hydroxyl (TOH), while the other hydrogen from the water molecule binds to a doubly coordinated bridging oxygen and forms a bridging hydroxyl (BOH). The ab initio derived elementary structure of the fully hydroxylated rutile cell ($l_x = 5.918 \text{ \AA}$, $l_y = 6.497 \text{ \AA}$)⁴⁰ was replicated periodically in both x and y directions to produce a neutral hydroxylated surface with the dimension of $47.34 \times 51.98 \text{ \AA}^2$. The desired negatively charged hydroxylated surface in this paper was obtained from the above neutral surface by removal of a selected number of the bridging hydrogens (H_{BOH}); in this case, the percentage of deprotonated bridging oxygens (O_{BO}) determines the surface charge density. Therefore, 25% of the H_{BOH} atoms were removed from the fully hydroxylated surface, creating a charge density of -0.208 C/m^2 , which corresponds to pH ~ 7.8 (close to the physiological pH) in our simulations. The distribution of surface groups (the deprotonated sites: O_{BO}; the protonated sites: TOH and BOH) is shown in Figure 1a, with a pattern allowing maximum separation of like-charged groups.

The systems, consisting of the rutile surface and the RGD peptide, were solvated with 2194 SPC/E water molecules in a simulation box with the height of 50 Å. The protonation/deprotonation states of the ionizable residues were chosen on the basis of the pK_a of the isolated amino acids and the desired pH ~ 7.80 in our simulations. As shown in Figure 1b, the side chains of Arg (pK_a 12.0) and Asp (pK_a 3.90) were considered ionized, thus carrying a net positive charge and a net negative charge, respectively. The blocking group ACE was added to the N-terminus of the RGD and the blocking group NME was added to the C-terminus to mimic a peptide bond to account for the continuation of the peptide sequence. As in previous work,²² RGD with both Arg and Asp side chains H-bonded to the surface in a ‘horseshoe’ configuration^{15,41} (Figure 1c) was chosen to be the starting state. The γ-COO⁻ group of Asp residue was initially located in close proximity to one of the deprotonated O_{BO} (inset in Figure 1c); thus only one hydrogen bond existed between the COO⁻ and the H_{BOH}. A cation was positioned in the vicinity of the COO⁻ group at the beginning of the simulation (inset in Figure 1c). The electroneutrality of the entire system was achieved by a surplus of divalent (Mg²⁺, Ca²⁺, or Sr²⁺) or monovalent (Na⁺, K⁺, or Rb⁺) cations in the solution. Table 1 gives the Lennard-Jones (LJ) potential parameters, radii, and numbers of ions used in the simulation systems (one species of cation in each system).

Table 1. LJ Parameters, Radii, and Numbers of Ions Used in the Simulation Systems

ion	σ_{ion} (Å)	ϵ_{ion} (kcal/mol)	R_{ion}^a (Å)	no. of ions
Mg ²⁺	1.398 ^b	0.875 ^b	0.70 ± 0.04	24
Ca ²⁺	2.895 ^c	0.1 ^c	1.03 ± 0.05	24
Sr ²⁺	3.314 ^c	0.1 ^c	1.25	24
Na ⁺	2.584 ^d	0.1 ^d	0.97 ± 0.06	48
K ⁺	3.332 ^d	0.1 ^d	1.41 ± 0.08	48
Rb ⁺	3.528 ^d	0.1 ^d	1.50	48
Cl ⁻	4.401 ^c	0.1 ^c	1.80 ± 0.07	16

^aThe calculated ionic radii in solution from ref 42. ^bFrom ref 43. ^cFrom ref 44. ^dFrom ref 45.

The LAMMPS package⁴⁶ was employed to perform MD simulations of the interfacial interactions in the RGD/rutile/aqueous solution system. The AMBER force field⁴⁷ was adopted to adequately represent peptide structures and the interaction potentials involving the rutile atoms were obtained from the literature.^{48,49} All of the MD simulations were performed in the NVT ensemble using the Nosé-Hoover thermostat.⁵⁰ Periodic boundary conditions were applied in the *x* and *y* directions, and a reflecting boundary condition was applied in the *z* direction. The coordinates of the atoms on and below the Ti–O plane (indicated in Figure 1c) were kept frozen. The surface atoms above the Ti–O plane were flexible; however, the Ti–O bonds (only for the terminal oxygen (O_{TOH}) and the O_{BO}) and O–H bonds (for the surface hydroxyls) were constrained using the SHAKE algorithm.⁵¹ Long-range electrostatic interactions were implemented with the standard Ewald summation, with a real space cutoff of 12 Å. The equations of motion were integrated using a time step of 2 fs, with coordinates saved every 3 ps.

Each system was subjected to an equilibration protocol; initially, the coordinates of RGD were frozen in the starting position to randomize the position of the solvent (water and ions) without disrupting the ‘horseshoe’ configuration of the peptide. After an energy minimization (corresponding to approximate 0 K), solute constraints were removed and the temperature of the system was increased gradually from 0 to 300 K in increments of 50 K every 40 ps.^{15,22} Finally, a typical 6 ns production simulation, at 310 K, was performed for each molecular assembly.

2.2. Structural and Dynamical Characterizations. Pair correlation function, coordination number, self-diffusion coefficient, and residence time were selected as the descriptors for the global structural and dynamical properties of the ions.

2.2.1. Coordination Number. We are interested in particles *i* that are ions and particles *j* that are waters. The space around the particle *i* from the value of r_0 , where the pair correlation function $g_{ij}(r)$ just becomes nonzero before its first peak, to the value of r_{fmin} , where $g_{ij}(r)$ reaches its first minimum, is called the first hydration shell of ion *i*. The integral of $g_{ij}(r)$ up to r_{fmin} yields a value for the first coordination number (n_{CN})⁵²

$$n_{\text{CN}} = 4\pi \int_{r_0}^{r_{\text{fmin}}} r^2 g_{ij}(r) \rho \, dr \quad (1)$$

2.2.2. Self-Diffusion Coefficient. The ionic mobility will be discussed in terms of self-diffusion coefficient (D), which is obtained by monitoring the mean square displacement of the ion and exploiting the well-known relation⁵³

$$D = \frac{1}{6} \lim_{t \rightarrow \infty} \frac{d}{dt} \langle |R(t) - R(0)|^2 \rangle \quad (2)$$

where $R(t)$ and $R(0)$ denote the coordinates of the ion at time *t* and at the reference time, respectively.

2.2.3. Residence Time. The residence time correction function of the first hydration shell of the ion is defined by⁵³

$$R(r, t) = \frac{1}{N_p} \sum_{i=1}^{N_p} \frac{1}{N_r} \sum_{j=1}^{N_r} [\theta_{ij}(r, t) \theta_{ij}(r, 0)] \quad (3)$$

where $\theta_{ij}(r, t)$ is the Heaviside unit step function, which is 1 if a water molecule *j*, originally in the spherical region of radius *r* (within the first hydration shell of ion *i*), remains in this region at time *t* and 0 otherwise. N_r is the number of water molecules around ion *i* in the spherical region of radius *r* at *t* = 0, N_p is the total number of the involved ions. The characteristic decay time (residence time), τ , is obtained by fitting the time correction function to an exponential decay

$$R(r, t) \approx \exp(-t/\tau) \quad (4)$$

The residence time τ will be considered to be infinity (∞), if $\theta_{ij}(r, t)$ always equals 1 during the entire sampling time.

3. RESULTS AND DISCUSSIONS

The structural and dynamical properties of bulk cations, as well as the binding modes of cations at the rutile/water interface, will be discussed to help to understand the effect of mediating cations on the adsorption of the negatively charged Asp side chain onto the negatively charged hydroxylated rutile (110) surface. The repulsion between the adsorbed cations and the positively charged Arg side chain will not be the focus of this paper, and will be discussed in future work. The role of Cl⁻ ions in peptide/rutile binding will not be evaluated in detail, since the anions do not directly adsorb or approach closely to the negatively charged surface, thereby having little impact on the peptide/rutile interaction. O_w, O_{TOH}, and O_{BOH} refer to oxygens in water, TOH and BOH groups, respectively, and H_w, H_{TOH}, and H_{BOH} refer to hydrogens in water, TOH and BOH groups, respectively. O_{OH} and H_{OH} are the generic terms for hydroxyl oxygens (O_{TOH} and O_{BOH}) and hydroxyl hydrogens (H_{TOH} and H_{BOH}), respectively. Bridging oxygen is the generic term for O_{BO} and O_{BOH}.

3.1. Bulk Properties of Cations. As will be confirmed, cation–oxygen interaction plays a major role in determining the nature of the binding of adsorbed cations. The ion–oxygen pair correlation function $g_{\text{ion-O}}$ for the fully solvated bulk ions is shown in Figure 2, and the ionic properties are summarized

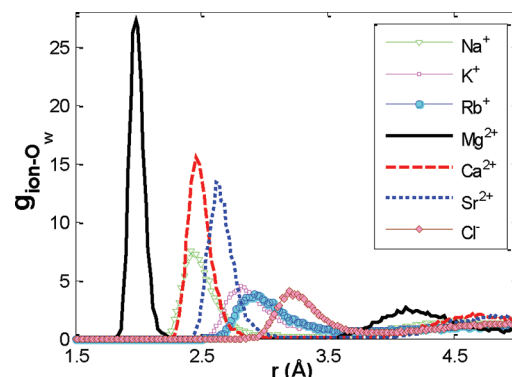


Figure 2. Pair correlation functions between the ions and the oxygens of water molecules in the bulk solvent phase.

in Table 2. The position of the first peak (r_{fmax}) of $g_{\text{ion-O}}$, which is the most probable separation of the center of an ion in the bulk from the centers of oxygens of surrounding water molecules, accords well with the mean ion–water internuclear distance ($d_{\text{ion-w}}$) from an extensive review⁴² on the basis of

Table 2. Structural and Dynamical Properties of Bulk Cations

ion	$r_{f\max}$ (Å)	$g_{f\max}$	$r_{f\min}$ (Å)	$d_{\text{ion-w}}^a$ (Å)	n_{CN}	τ (ps)	D ($10^{-5} \text{ cm}^2 \cdot \text{s}^{-1}$)	D^b ($10^{-5} \text{ cm}^2 \cdot \text{s}^{-1}$)
Mg ²⁺	1.98	27.19	2.32	2.090±0.041	6.00 (6) ^c	∞	0.64	0.706
Ca ²⁺	2.46	15.50	3.02	2.422±0.052	7.93 (8.0, 8.2) ^d	485.44	0.68	0.792
Sr ²⁺	2.62	13.36	3.18	2.64±0.04	8.30 (7.9) ^d	158.77	0.84	0.791
Na ⁺	2.42	7.55	3.25	2.356±0.060	5.78 (6) ^e	22.24	1.67	1.334
K ⁺	2.82	4.56	3.66	2.798±0.081	7.03 (6, 8) ^{f,g}	9.60	2.47	1.957
Rb ⁺	2.92	3.73	3.82	2.89	7.60	6.34	2.63	2.072

^aThe mean ion–water internuclear distance from ref 42. ^bThe self-diffusion coefficient from ref 54. ^cFrom ref 55. ^dFrom ref 56. ^eFrom ref 57. ^fFrom ref 58. ^gFrom ref 59.

numerous studies. Treating the involved cations with the same charge as a separate series, we can find that within each series (monovalent or divalent), the values listed in Table 2 vary with the size of cations (indicated by arrows). The amplitude of the first peak in $g_{\text{ion-Ow}}$ ($g_{f\max}$) becomes weaker with increasing ionic size, but the calculated first coordination numbers (n_{CN}), comparable to the experimental results (quantities in parentheses), show an opposite trend. The dynamics of the cations and the tightness of the first hydration shell can be characterized by the self-diffusion coefficient (D) and the residence time (τ). The values of D listed in Table 2 are broadly consistent with a published simulation work.⁵⁴ The existing differences may derive from the differences in the force field, temperature and size of the two systems. The values of τ for the first hydration shell of both monovalent and divalent cations decline rapidly with increasing ion size, while the values of D for cations increase with increasing ion size. Moreover, τ for the divalent cations is larger than the value for the monovalent cations by at least a factor of 7, and D for the divalent cations is almost half of the value for the monovalent cations.

From the above information, we may infer that significant exchange of water molecules in the first hydration shell around the monovalent cations with the surroundings can occur in a very short time; that is, the first hydration shell around the monovalent cations breaks and reforms constantly (see residence time in Table 2, $\tau < 25$ ps). However, the divalent cations move together with the hydration shell, a situation that makes their dynamics slower than the monovalent cations. This is especially the case for Mg²⁺ ions, with its small radius. The water molecules in the first hydration shell adhere strongly to Mg²⁺ and move with it as a rigid unit. We may, therefore, expect that the Mg²⁺ ions can form strong, direct bonds with the surroundings, including water molecules and peptide atoms. However, the ion–water binding is a much more dynamical process for monovalent cations than divalent cations; thus the bonds between the monovalent cations and the peptide atoms (if present) may also be temporary, because the monovalent cations will form a weaker interaction with the peptide atoms just as they form weaker interactions with the surrounding waters.

3.2. Adsorption of Cations at the Water/Rutile Interface. The ions can adsorb at inner- and outer-sphere binding configurations and these are shown in Figure 3. The inner-sphere species can adsorb at three different sites on the surface, including a tetradentate site (TD: two O_{TOH} and two bridging oxygens, Figure 3a), and two bidentate sites (BD-BOTO: one O_{TOH} and one bridging oxygen, Figure 3b; BD-TOTO: two O_{TOH}, Figure 3c). The axial densities of cations, as a function of distance from the surface in Figure 4 (a: monovalent cations; b: divalent cations), are calculated from

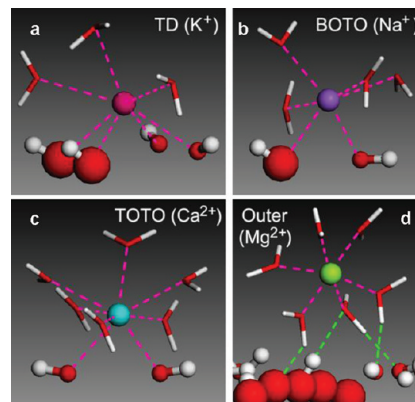


Figure 3. Representative inner- and outer-sphere binding configurations of the adsorbed cations. (a) TD (K⁺), (b) BD-BOTO (Na⁺), (c) BD-TOTO (Ca²⁺), and (d) outer-sphere (Mg²⁺). The hydrogen bonds and direct bonds (connected to the cations) are represented by green and magenta dashed lines, respectively.

the atoms at narrow bins of width, $\Delta z = 0.04$ Å. The zero height (i.e., $z = 0$) is set to the position that the surface layer of Ti atoms would occupy in the unrelaxed crystal termination and will hereafter be called ‘rutile plane’. The properties of cations located outside the RGD region (Figure 4c, the space above the surface occupied by the entire RGD peptide) will be analyzed in detail in this section. Table 3 gives the binding distances of cations from the rutile plane, the occupancies of available adsorption mode (the percentage of adsorbed cations in a given adsorption site relative to the total number of cations in the region 0–7 Å from the rutile plane), and the weighted average binding distances (the sum of occupancies multiplied by their binding distances). The data in Figure 4 and Table 3 will be discussed below.

3.2.1. Monovalent Cations. The small occupancies of the outer-sphere binding mode for Na⁺, K⁺, and Rb⁺ (<3.10%, Table 3) show that there is less than one outer-sphere monovalent cation on the entire surface at a given point in time, occurring when one or two cations temporarily penetrate into the outer-sphere region. The involved monovalent cations can, therefore, be considered to exclusively adsorb on the negatively charged hydroxylated rutile (110) surface at the inner-sphere binding sites. The axial density profile of Na⁺ (shown in Figure 4a) exhibits a first sharp peak at $z = \sim 3.04$ Å, indicating that more than half of Na⁺ ions adsorb at TD sites. The small shoulder ($z = \sim 3.49$ Å) and the second peak ($z = \sim 3.78$ Å) represent a minority of Na⁺ adsorbing at BD-BOTO and BD-TOTO sites, respectively. For the adsorbed K⁺ and Rb⁺ ions at the water/rutile interface, the TD mode is more

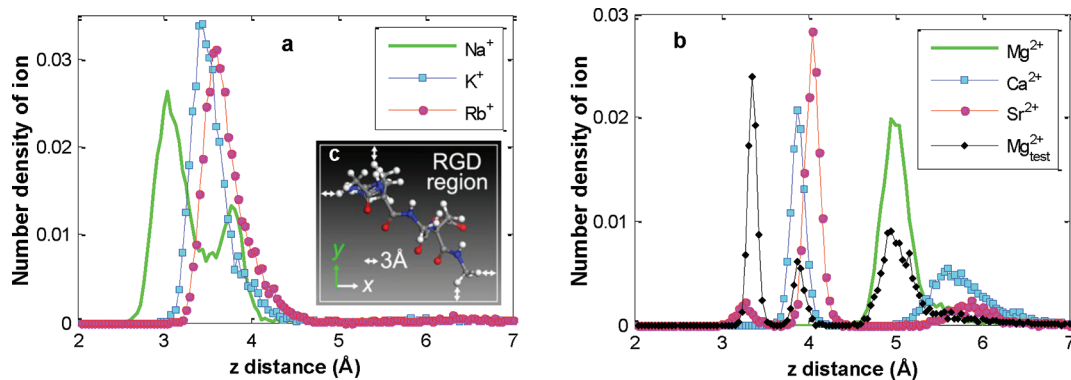


Figure 4. Axial density profile of cations on the negatively charged hydroxylated rutile (110) surface. (a) Monovalent cations, (b) divalent cations, and (c) the geometry of the region occupied by RGD.

Table 3. Binding Configurations, Occupancies, Distances, and Weighted Average Distances (above the Rutile Plane) of Cations on the Negatively Charged Hydroxylated Rutile (110) Surface

ion	inner-sphere				outer-sphere				weighted avg. <i>h</i> (Å)
	TD		BD-BOTO		BD-TOTO				
	<i>h</i> (Å)	occup (%)							
Mg ²⁺		0		0		0	5.07	100	5.07
Ca ²⁺		0		0	3.87	49.91	5.76	50.09	4.82
Sr ²⁺	3.26	6.31		0	4.05	77.35	5.92	16.34	4.31
Na ⁺	3.04	57.61	3.49	12.71	3.78	27.42	5.86	2.26	3.36
K ⁺	3.48	84.53	4.00	8.99	4.38	4.19	6.11	2.29	3.62
Rb ⁺	3.63	82.39	4.15	9.21	4.39	5.35	6.23	3.05	3.80

predominant as indicated by larger occupancies (>80%, Table 3).

3.2.2. Divalent Cations. The axial density profile of Mg²⁺ with a peak centered at 5.07 Å (Figure 4b) indicates complete outer-sphere binding. The charge of +2e and the small radius contribute to a strong tendency of Mg²⁺ to stay fully solvated at the water/rutile interface. A simulation with Mg²⁺ ions initially positioned at different distances from the rutile plane was performed to test the possibility of other binding geometries of Mg²⁺ on the negatively charged hydroxylated rutile (110) surface. A portion of Mg²⁺ ions were put close to the surface (within 3–4 Å distance from the rutile plane) to artificially allow the inner-sphere binding, while others are positioned far away from the surface (>8 Å). As seen in Figure 4b (black curve), the inner-sphere binding Mg²⁺ ions split into two different species. The first sharp peak refers to the ions adsorbing at the BD-TOTO sites, while the second small peak is formed by a minority of Mg²⁺ ions located above a single O_{TOH}. However, the inner-sphere binding Mg²⁺ ions show no tendency to diffuse into the outer-sphere region on the present time scale, while the Mg²⁺ ions adsorbed at the outer-sphere sites (from bulk) indicate no trend to penetrate into the inner-sphere region or the bulk solvent space. It can be inferred that even though Mg²⁺ ions are stable at both inner- and outer-sphere binding sites, there seems to be a large energy barrier hindering the interchange of Mg²⁺ between these two regions. Once the first hydration shell is formed around the Mg²⁺, the connections between these water molecules and the center cation will be extremely stable due to a short Mg²⁺–O_w direct bond (1.98 Å). Similarly, the direct bonds between the Mg²⁺ and the surface oxygens, which ‘trap’ the cation at the adsorption site, are also difficult to disrupt, if the initial position of the cation allows the inner-sphere binding.

In contrast from Mg²⁺, Ca²⁺ ions adsorb in equal amounts at the BD-TOTO sites and the outer-sphere sites on the desired rutile surface (Table 3). Although the interchange of Mg²⁺ ions between the inner- and outer-sphere regions may occur on a larger time scale, the present results indicate that the kinetic hindrance for transition between inner- and outer-sphere binding geometries is much larger for the Mg²⁺ ions than for the Ca²⁺ ions, which will significantly affect the mediation mode of cations in peptide/rutile binding. The BD-TOTO binding geometry predominates for the adsorbed Sr²⁺ ions, with a minority of TD and outer-sphere binding species (Table 3). An interesting question to be clarified is why the BD-TOTO is the main site for the inner-sphere binding of divalent cations. As stated in previous work,²² the O_{TOH} shows a stronger attraction for the positively charged species than the O_{BOH}; thus it makes sense that a doubled electrostatic attraction between the O_{TOH} and the divalent cations (compared with the case for the monovalent cations) tends to “trap” the cations at the BD-TOTO sites.

3.2.3. Discussion of Cation Adsorption at the Water/Rutile Interface. Cation desolvation is expected to be much easier for the involved monovalent cations than the divalent cations in part because the hydration waters are bound much more tightly to the latter (see τ in Table 2), which should result in differences in the adsorption mode of cations between the two series. The adsorption of cation at a TD site requires the removal of four tightly bound waters in the first hydration shell. Monovalent cations with a relatively loose hydration shell are more readily desolvated, thereby resulting in a predominance of the TD mode in the adsorption of Na⁺ (57.61%), K⁺ (84.53%), and Rb⁺ (82.39%). In contrast, the removal of two primary hydration waters to vacate the sites for the BD-TOTO binding is relatively more favorable for Ca²⁺ (49.91%) and Sr²⁺

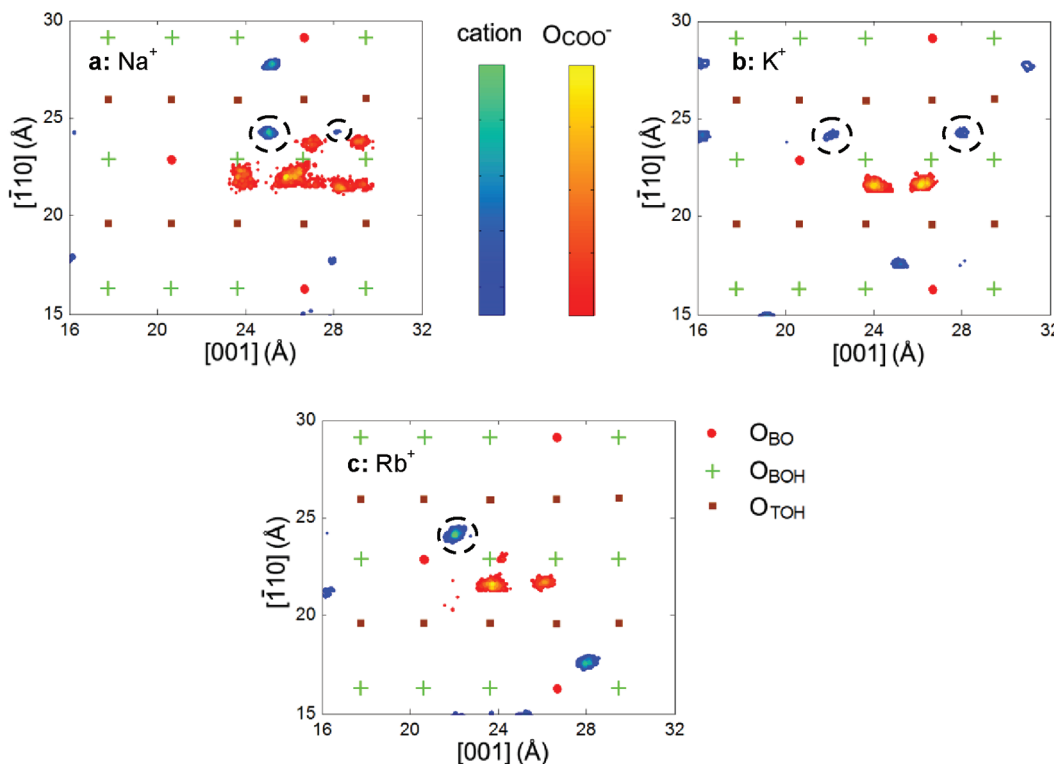


Figure 5. 2D density maps of the adsorbed monovalent cations and the COO^- group on the negatively charged hydroxylated rutile (110) surface during the final 2 ns of simulation. (a) In NaCl , (b) in KCl , and (c) in RbCl . Color codes: O_{BO} , red dot; O_{BOH} , green plus; O_{TOH} , brown square. The mediating cations are labeled by black dashed circles.

(77.35%) with a tighter hydration shell. It can be inferred that the desolvation of divalent cations in the order $\text{Sr}^{2+} > \text{Ca}^{2+} > \text{Mg}^{2+}$ (easy-to-hard, inferred from τ and the occupancies) will contribute to the electrostatic attraction existing between the cation and the negatively charged surface atoms or the negatively charged peptide group, thereby affecting the binding strength of cation-surface or cation-peptide complex.

Monovalent cations bind to the surface oxygens directly without the mediation by hydration waters; thus the distances between the binding sites and the adsorbed cations mainly depend on the ionic radii. However, the outer-sphere binding divalent cations with their hydration shells exhibit a larger solvated ionic radius, i.e., effective radius. Therefore, the weighted average height of adsorbed cations was introduced to characterize the adsorption strength of different cations on the negatively charged hydroxylated rutile (110) surface. This is because the larger the weighted average height of cations from the surface, the weaker the electrostatic attraction for the surface oxygens (indicating a weaker adsorption strength). For the adsorbed monovalent cations, the weighted average heights in the order $\text{Rb}^+ > \text{K}^+ > \text{Na}^+$ (Table 3) exhibit a ‘reverse’ lyotropic trend of adsorption strength with decreasing crystallographic radii. In contrast, the weighted average heights of adsorbed divalent cations on the same surface in the order $\text{Mg}^{2+} > \text{Ca}^{2+} > \text{Sr}^{2+}$ is consistent with a “regular” lyotropic trend, i.e., the adsorption strength of divalent cations increases with increasing crystallographic radii. To the best of our knowledge, comprehensive experimental results covering all the involved cations on the TiO_2 surface have not been reported previously. However, the same “reverse” lyotropic trend of the monovalent cations (Li^+ , K^+ , and Cs^+) on the rutile surface (i.e.,

the adsorption affinity following the sequence: $\text{Li}^+ > \text{K}^+ > \text{Cs}^+$) has been observed in many experimental studies.^{28,29,31}

3.3. Cation Mediation in Asp/Rutile Binding. The charge screening of cations, which overcomes the electrostatic double-layer repulsion between the negatively charged adsorbate and the negatively charged adsorbent, has been highlighted in many experimental studies of the adsorption of negatively charged nucleic acids on the negatively charged mineral surfaces.^{23–27} Thus, it would be interesting to analyze how the cations with different charges and ionic radii mediate and regulate the adsorption of a negatively charged Asp residue on the negatively charged rutile surface. In the present simulations, the COO^- group is H-bonded to the surface through one O_{COO}^- , while the other O_{COO}^- is close to a deprotonated O_{BO} without H_{BOH} available for a hydrogen bond (Figure 1c). A TD cation was initially positioned in the vicinity of the COO^- group (inset in Figure 1c), and will be subsequently called the “preadsorbed” cation. Since the monovalent cations adopt the inner-sphere binding modes far more frequently than the outer-sphere modes, in the following sections, we will only discuss the inner-sphere mediation by monovalent cations in Asp/rutile binding. However, both the inner- and outer-sphere mediation modes of the divalent cations will be analyzed because the outer-sphere binding geometry prevails in the Mg^{2+} and Ca^{2+} ions when they move toward the surface from the bulk and finally adsorb on the negatively charged hydroxylated rutile surface.

3.3.1. Inner-Sphere Mediation by Monovalent Cations. Since one of the O_{COO}^- atoms in the simulation systems is initially close to the O_{BO} without an attached H_{BOH} , the lateral movement or the rotation of COO^- group is the only way to form enough hydrogen bonds with the surface. To visualize the

positions of the COO^- group and the adsorbed compensating cations on the surface, 2D density maps within the region $16 \leq x \leq 32$, $15 \leq y \leq 30$ for systems with monovalent cations (Na^+ , K^+ , or Rb^+) during the final 2 ns of simulation are displayed in Figure 5 (the mediating monovalent cations are labeled by black dashed circles). As expected, the COO^- group moves along the [001] direction to leave the initially nearby O_{BO} atom, and keeps close to the adjacent BOH groups to form enough hydrogen bonds. However, the behavior of COO^- group and the mediation stability of cations are slightly different in the three systems.

As indicated in the 2D density map (Figure 5a), a TD-adsorbed compensating Na^+ ion remains close to the Asp side chain during most of the final 2 ns, participating in bridging the COO^- group to the surface; however, the COO^- group in the NaCl solution exhibits a less localized density, indicating multiple positions in the [001] direction (a range from 23.5 to 30 Å). In contrast, the COO^- groups in KCl and RbCl solutions are almost anchored to the surface, remaining in the same position during the final 2 ns of simulation (KCl: from 23.5 to 27 Å, Figure 5b; RbCl: from 23 to 26.5 Å, Figure 5c). A TD-adsorbed Rb^+ (labeled by a dashed circle) keeps in close proximity to the Asp side chain, actively involved in Asp/rutile adsorption. Two TD-adsorbed K^+ ions approach the COO^- group, acting as a bridge between the negatively charged Asp side chain and the negatively charged rutile surface; however, the mediating K^+ ions cannot remain stably in the vicinity of the COO^- group, which is indicated by the small blue regions (labeled by dashed circles) in Figure 5b.

To find out how far the Asp side chain is from the surface when mediated by different cations, we calculated the mean value (μ) and the standard deviation (σ) of distances between the O_{COO}^- atoms and the rutile plane in the direction perpendicular to the surface during the final 2 ns of simulation (see Table 4). The COO^- group in both NaCl and KCl

Table 4. Distances from the O_{COO}^- to the Rutile Plane in the Direction Perpendicular to the Surface

solution	O_{COO}^- -1		O_{COO}^- -2	
	μ (Å)	σ (Å)	μ (Å)	σ (Å)
NaCl	3.50	0.27	3.68	0.22
KCl	3.56	0.17	3.63	0.15
RbCl	4.22	0.73	3.83	0.56
MgCl_2	4.78	0.09	5.80	0.45
CaCl_2	5.26	0.24	6.31	0.20
SrCl_2	5.87	0.22	4.95	0.16

solutions stays close to the surface in a stable configuration ($\mu < 3.70$ Å, $\sigma < 0.30$ Å), forming enough hydrogen bonds with the surface hydroxyls to remain attached, as shown in the

representative configurations (Figure 6a and 6b). In contrast, the deviations of the COO^- -rutile distances ($\sigma > 0.50$ Å) are much larger in the RbCl solution, which results from the state switching between the two O_{COO}^- atoms. In the representative configuration of the molecular assembly (Figure 6c), both O_{COO}^- atoms can form a direct bond with the mediating Rb^+ ion, but only one O_{COO}^- is involved in H-bond connection with the surface. Thus two O_{COO}^- atoms can rotate around the $\text{C}_\beta-\text{C}_\gamma$ direction ($\text{C}_\beta, \text{C}_\gamma$ in the Asp side chain, Figure 1b) and switch their states, which explains the coexistence of a larger deviation of the COO^- -rutile distances and a localized density of the COO^- group. In summary, the Asp side chain in NaCl, KCl and RbCl solutions stays attached to the surface by the combined effect of two factors, i.e., cation mediation and H-bond connections with the surface (mainly represented by the $\text{H}_{\text{BOH}}\cdots\text{O}_{\text{COO}}^-$ hydrogen bonds). However, the direct bonds between the O_{COO}^- atoms and the mediating monovalent cations sometimes break as a result of the lateral motion of COO^- group (e.g., in NaCl solution) or the diffusion of cations (e.g., in KCl solution).

3.3.2. Inner-sphere mediation by divalent cations. Figure 7 gives the 2D density maps representing the positions of the adsorbed divalent cations and the COO^- group of RGD during the final 2 ns of simulation. The COO^- -surface binding sites (labeled by magenta dashed rectangles) are magnified in the insets (1: Mg^{2+} ; 2: Ca^{2+} ; 3: Sr^{2+}). As indicated in Table 4 ($\mu > 4.50$ Å), the COO^- group in the systems with divalent cations (Mg^+ , Ca^+ , or Sr^+) stays farther away from the surface, thereby losing H-bond connections with the rutile atoms. However, the Asp side chain shows less mobility and remains on the binding site, which can be inferred from the localized density of the COO^- group (Figure 7). This is because an adsorbed divalent cation (labeled by black dashed circles in the insets of Figure 7) stays in close proximity to the COO^- group stably, helping to bridge the Asp side chain to the rutile surface. As will be confirmed, the preadsorbed divalent cation is the one always staying together with the Asp side chain. To monitor the Asp/cation/rutile interaction, Figure 8 displays the distances from the preadsorbed divalent cations (denoted by the subscript “-1”) to the COO^- group, as well as the z position of this specific cation with respect to the rutile plane. The initial time segment, labeled by markers (square, circle, and cross), refers to the evolution of distances during the temperature rise stage (280 ps), and the rest of the curves correspond to the production run (6 ns).

As shown in Figure 8, panels a and b (black curves—the z distance of cation to the rutile plane), the preadsorbed TD Mg^{2+} -1 and Ca^{2+} -1 move away from the surface, finally staying at a BD-TOTO site with a height of ~3.40 Å and ~3.85 Å, respectively. Unlike them, the preadsorbed Sr^{2+} -1 stays at the original TD site (black curve in Figure 8c), because the Sr^{2+}

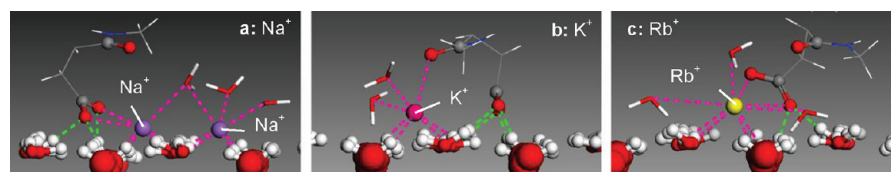


Figure 6. Configurations of part of the molecular assembly at $t = 6$ ns. (a) Na^+ , (b) K^+ , and (c) Rb^+ . The O_{BOH} and O_{BO} are shown in CPK representation (large spheres); the H_{BOH} , TOH, COO^- , CO, and the adsorbed cations are shown in ball-and-stick representation; and the involved hydration waters are shown in stick representation. The hydrogen bonds and direct bonds (connected to the cations) are represented by green and magenta dashed lines, respectively.

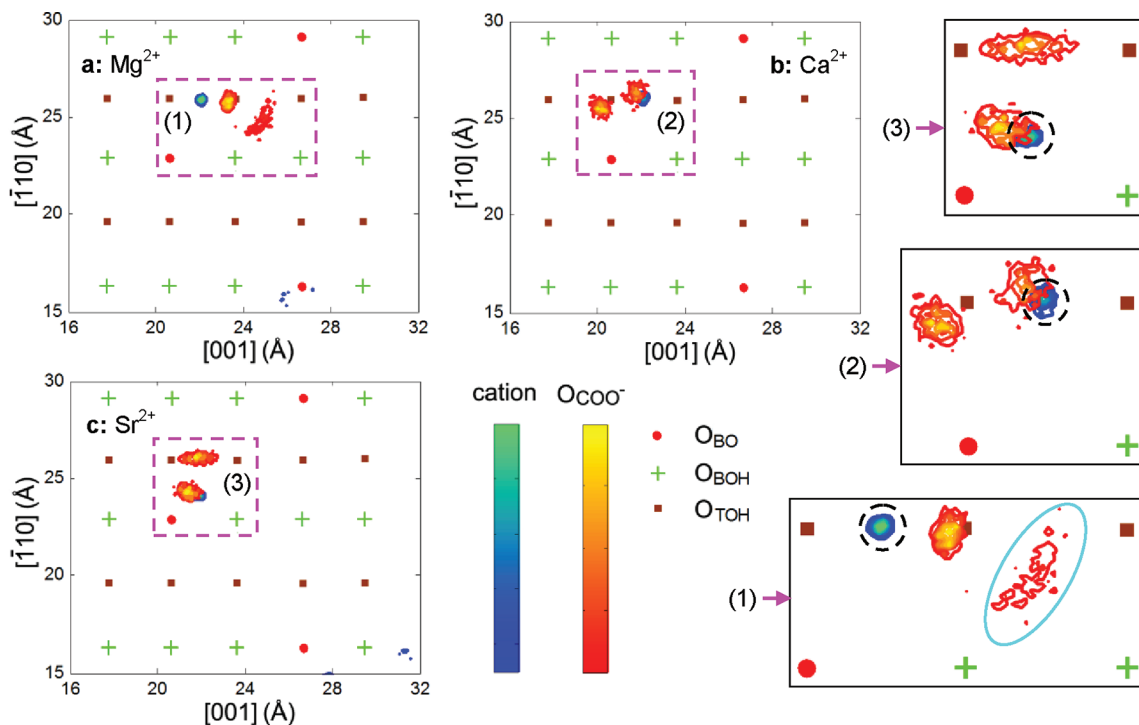


Figure 7. 2D density maps of the adsorbed divalent cations and the COO^- group on the negatively charged hydroxylated rutile (110) surface during the final 2 ns of simulation. (a) In MgCl_2 , (b) in CaCl_2 , and (c) in SrCl_2 . The binding sites are magnified in the insets. Color codes: O_{BO} , red dot; O_{BOH} , green plus; O_{TOH} , brown square. The mediating cations are labeled by black dashed circles.

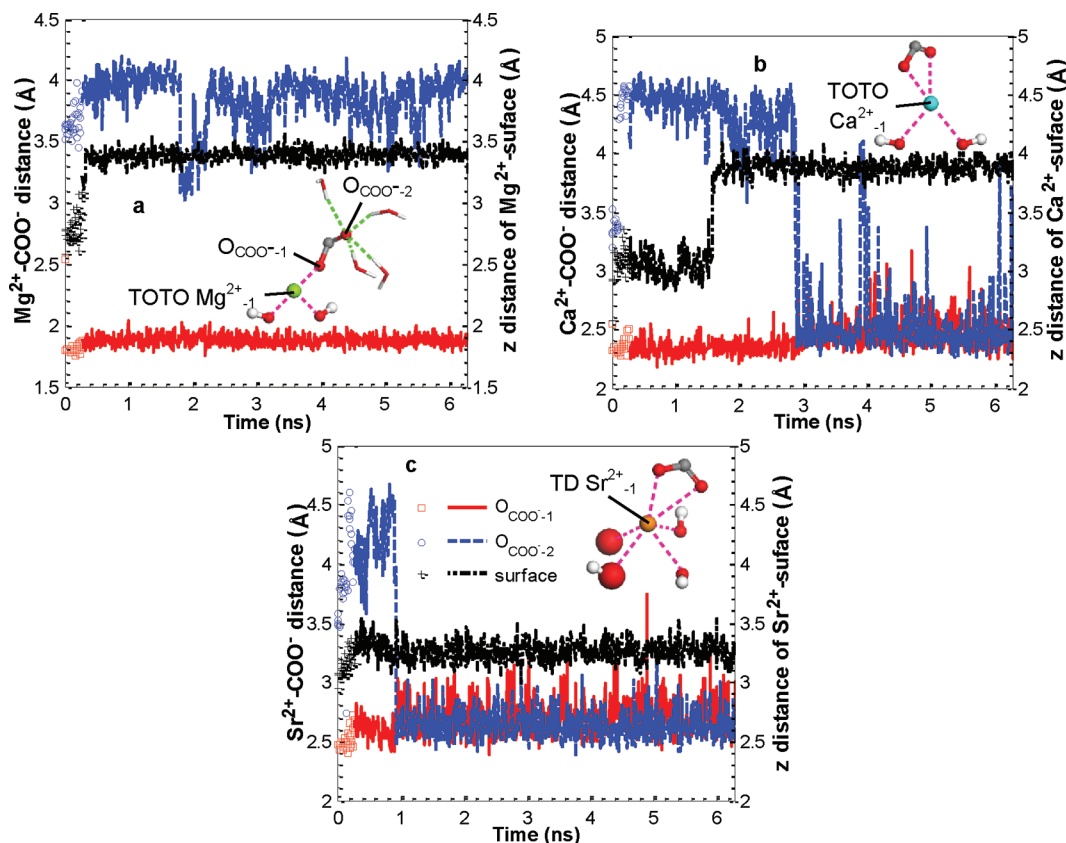


Figure 8. Evolution of the distances from the preadsorbed divalent cations to the COO^- group, as well as the z -position of these specific cations with respect to the rutile plane. (a) Mg^{2+}_{-1} , (b) Ca^{2+}_{-1} , and (c) Sr^{2+}_{-1} . The initial time segment labeled by markers (square, circle, and cross) refers to the evolution of distances during the temperature rise stage (280 ps), and the rest of the curves correspond to the production run (6 ns).

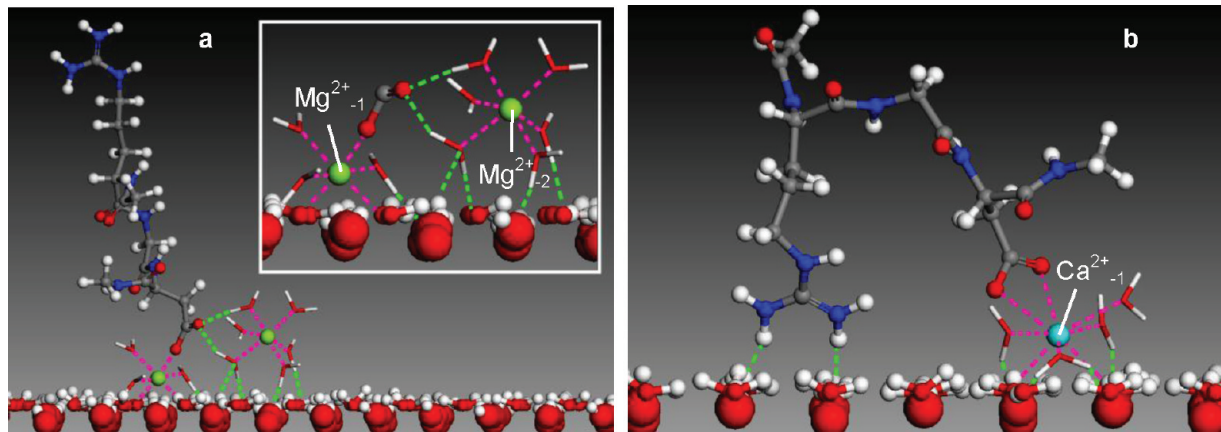


Figure 9. Adsorption configurations of RGD on the rutile surface at $t = 6$ ns. (a) In MgCl_2 and (b) in CaCl_2 . The O_{BOH} and O_{BO} are shown in CPK representation (large spheres), the H_{BOH} , TOH, RGD and the adsorbed cations are shown in ball-and-stick representation, the involved hydration waters are shown in stick representation. The hydrogen bonds and direct bonds (connected to the cations) are represented by green and magenta dashed lines, respectively.

ions are capable of adsorbing on the negatively charged hydroxylated rutile (110) surface at the TD, BD-TOTO, and outer-sphere binding sites (see Table 3). In the MgCl_2 solution, the Asp side chain stays on the rutile surface stably with one O_{COO^-} bound to the preadsorbed Mg^{2+}_{-1} and the other O_{COO^-} free to interact with the surrounding waters (snapshot in Figure 8a). The O_{COO^-} atom not involved in any direct interaction with the mediating cation or the surface atoms moves around the other O_{COO^-} atom, which is almost ‘trapped’ on the binding site via the mediation by Mg^{2+}_{-1} , resulting in a comparatively less localized density (labeled by the cyan circle in Figure 7-(1)). In the CaCl_2 and SrCl_2 solutions, the COO^- group moves farther away from the rutile surface and locates above the preadsorbed cation, with both O_{COO^-} atoms bound to the mediating BD-TOTO Ca^{2+}_{-1} (snapshot in Figure 8b) or the mediating TD Sr^{2+}_{-1} (snapshot in Figure 8c). The mediation by divalent cations reported here is comparable to the results obtained by Monti et al.⁶⁰ on the binding mode of the mediating cation and the mobility of the negatively charged COO^- group. In their simulations, a negatively charged partially hydroxylated rutile (110) surface originating from the neutral nonhydroxylated surface was built by adding a selected number of TOH groups. Monti et al. found that the mediating Ca^{2+} adsorbed between two terminal oxygens, similar to the case of inner-sphere mediation by Mg^{2+} and Ca^{2+} in the present work. Moreover, the O_{COO^-} atom initially coordinated to a titanium site in the work of Monti et al. reoriented itself toward the mediating Ca^{2+} , with the separation of the O_{COO^-} atom from the original binding site increased to larger than 4 Å. Similarly, the COO^- group in the present work moved farther away from the originally H-bonded surface hydroxyls to form direct bonds with the mediating divalent cations. These data indicate that the divalent cations in the present work can compensate for both the carboxyl group and the surface charges, supporting the view that the adsorption of COO^- group on the negatively charged surface can occur via Mg^{2+} , Ca^{2+} , or Sr^{2+} acting as a bridge between the peptide and the surface.

At the end of the 6 ns production run, a configuration where one end of the molecule (COO^-) is attached to the surface and the other end (NH_2) is free in the solvent phase (Figure 9a) is presented in the system with Mg^{2+} ions. As shown in the inset of Figure 9a, in coordination with the mediation by the preadsorbed Mg^{2+}_{-1} , another cation from the bulk solvent

(denoted by Mg^{2+}_{-2}) approaches the free O_{COO^-} atom in a double outer-sphere configuration, i.e., the Mg^{2+}_{-2} is linked to the rutile surface and the O_{COO^-} atom via the intermediate water molecules at the same time. The simulation was extended to 9 ns to test the stability of the double outer-sphere mediation by Mg^{2+}_{-2} , which will be discussed below. Contrary to these findings for MgCl_2 , the RGD in the CaCl_2 solution finally presents a “horseshoe” configuration (Figure 9b). The two completely different configurations of RGD in Figure 9 will be used in the testing simulations of outer-sphere mediation by Mg^{2+} and Ca^{2+} in the following sections.

3.3.3. Discussion of Inner-Sphere Mediation. The above simulation results indicate that the Asp side chain, when RGD is in NaCl , KCl or RbCl solutions, remains H-bonded to the surface during the entire simulation. Meanwhile, the cations can approach the vicinity of the COO^- group, participating in bridging the negatively charged Asp side chain to the negatively charged surface. It is also suggested that the TD geometry is the unique adsorption mode of the mediating monovalent cations (Na^+ , K^+ , and Rb^+) in the Asp/rutile binding. However, the movement of COO^- group (e.g., in NaCl solution) or the diffusion of cations (e.g., in KCl solution) during the simulation sometimes results in breakdown of the direct bonds between the O_{COO^-} atoms and the mediating cations, which may be ascribed to two factors: i. Coordination saturation of the O_{COO^-} atom; since a large number of stable hydrogen bonds between the two O_{COO^-} atoms and the H_{OH} are capable of trapping the COO^- group on the surface, the mediating cation is not essential to the Asp/rutile binding. ii. Residence time of the particles (peptide atoms, surface atoms or waters) within the first neighborhood of the monovalent cations. The residence time τ listed in Table 2 shows that the waters can remain in the first hydration shell of monovalent cations for less than 30 ps before significant exchange with the surroundings occurs. That is, the direct bonds, from the Na^+ and K^+ ions to the water molecules, COO^- group or the surface oxygens are inherently weaker, and thus easily broken. In the case of RbCl solution, only one O_{COO^-} atom is involved in hydrogen bonds with the surface, which cannot be solely responsible for trapping the Asp side chain on the rutile. The COO^- group is, therefore, readily available for a direct bond with the preadsorbed Rb^+ to further stabilize itself on the surface.

Unlike the monovalent cations, the stronger attraction of the preadsorbed divalent cations (Mg^{2+}_{-1} , Ca^{2+}_{-1} , and Sr^{2+}_{-1}) for the negatively charged COO^- group, compared with the attraction from the surface H_{OH} , causes the O_{COO}^- atoms to move farther away from the surface to be located above the preadsorbed cation, thereby breaking the $H_{OH}\cdots O_{COO}^-$ hydrogen bonds. However, the Asp side chain remains stably on the surface during the entire simulation via the mediation by the preadsorbed inner-sphere divalent cations. That is, the link between the COO^- group and the surface provided by the mediating divalent cation is strong enough to “trap” the Asp side chain on the surface within the sampling time, even in the absence of H-bond connection between the Asp residue and the surface.

3.3.4. Analysis of Outer-Sphere Mediation by Mg^{2+} and Ca^{2+} . As mentioned in section 3.2.2, the Mg^{2+} ions (from bulk) adsorb on the negatively charged hydroxylated rutile (110) surface at the outer-sphere binding sites, while half of the adsorbed Ca^{2+} ions on the same surface adopt a similar binding mode. Thus it is necessary to test the probability of the outer-sphere mediation by Mg^{2+} and Ca^{2+} . The double outer-sphere mediation by Mg^{2+}_{-2} , mentioned in the end of section 3.3.2 (The simulation was extended to 9 ns), lasts for ~ 1.2 ns before the Mg^{2+}_{-2} ion leaves toward another outer-sphere site on the surface. This suggests that the Mg^{2+}_{-2} accompanied by its hydration shell is capable of bridging the peptide to the rutile surface in a double outer-sphere configuration; however, the mobility of Mg^{2+}_{-2} in the $x-y$ plane eventually leads to the breakdown of the COO^- ···water··· Mg^{2+}_{-2} ···water···rutile H-bond network.

In the following analysis, we focus on the single outer-sphere mediation by Mg^{2+} and Ca^{2+} , i.e., the cations are directly bound to the O_{COO}^- , but adsorbed on the surface as an outer-sphere species. The procedure for obtaining the molecular assemblies in the testing simulations is illustrated in Figure 10, where the

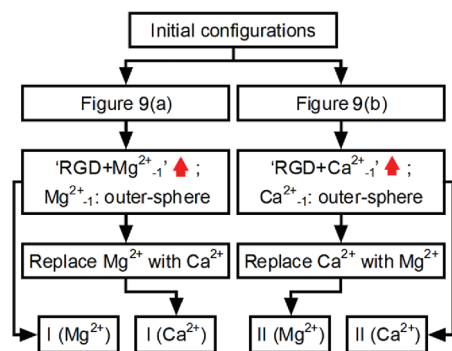


Figure 10. Schematic of the procedure for obtaining the molecular assemblies in the testing simulations. The red arrows denote that the $RGD+Mg^{2+}_{-1}$ (or $RGD+Ca^{2+}_{-1}$) complex was placed upward to allow the single outer-sphere mediation by Mg^{2+}_{-1} (or Ca^{2+}_{-1}), with the original interaction between the RGD and Mg^{2+}_{-1} (or Ca^{2+}_{-1}) retained.

red arrows denote that the RGD and the specific cations (Mg^{2+}_{-1} in Figure 9a; Ca^{2+}_{-1} in Figure 9b) were placed upward to allow the single outer-sphere mediation by Mg^{2+}_{-1} and Ca^{2+}_{-1} , with the original Mg^{2+}_{-1} -peptide or Ca^{2+}_{-1} -peptide interaction retained. The four resulting configurations were selected as the initial states of the testing assemblies, and the equilibration course was used as outlined in section 2.1 with a production run of 4.5 ns. The evolution of the distances from the single outer-sphere mediating Mg^{2+}_{-1} and Ca^{2+}_{-1} to the

COO^- group during the production run, as well as the z -position of these specific cations with respect to the rutile plane is shown in Figure 11 and 12.

In case I (Mg^{2+}) (Figure 11a), the predominant configuration of the COO^- group is one where one O_{COO}^- coordinates to the Mg^{2+}_{-1} ($Mg^{2+}_{-1}-O_{COO}^-$ distance = 1.86 ± 0.04 Å), while the other O_{COO}^- forms hydrogen bonds with the nearby water molecules. The RGD- Mg^{2+}_{-1} complex stays on the surface for longer than 2 ns, but finally moves freely in the solvent phase (Figure 11a-(2)). Unlike in case I, the single outer-sphere mediating Mg^{2+}_{-1} in case II (Ca^{2+}) (Figure 11b) keeps bridging both O_{COO}^- atoms to the rutile surface ($Mg^{2+}_{-1}-O_{COO}^-$ distance = 1.92 ± 0.06 Å). The Arg side chain is also bound to the surface and, therefore it is in a “horseshoe” configuration (Figure 11b-(1)) during the entire simulation. The initial state in case I is a configuration where Asp is attached to the surface but Arg is free in the solvent phase (Figure 9a), while the initial state in case II is a “horseshoe” configuration with both Arg and Asp attached to the surface (Figure 9b). We may speculate that in case I, the flexible Arg residue (not attached to the surface) moves freely in the solvent phase; thus the random diffusive motion causes the entire peptide to slowly move away from the surface. This is because the Arg in the solvent phase interacts with the surrounding waters actively, whereas the hydration waters of Mg^{2+}_{-1} are linked to the surface only through 2–4 hydrogen bonds. Compared to the extensive Arg-water hydrogen bonds, the H-bond connections between the hydration waters of Mg^{2+}_{-1} and the surface seems uncompetitive, thereby finally breaking (Figure 11a-(2)). However, in case II (Figure 11b-(1)), both the Arg side chain and the Asp- Mg^{2+}_{-1} complex were originally attached to the surface. The Arg-surface hydrogen bonds act as a restraining force, stabilizing the peptide on the surface rather than releasing it into the solvent. Thus, Mg^{2+}_{-1} in case I left the surface with the peptide, while the single outer-sphere Mg^{2+}_{-1} in case II remained on the surface, mediating the Asp/rutile binding. Hence, it may be inferred that the available Arg-surface hydrogen bonds help to keep the peptide on the surface, in coordination to the mediation by a single out-sphere Mg^{2+} . However, if the flexible Arg residue moves freely in the solvent phase and interacts actively with the surrounding waters, the peptide seems easy to be dragged away from the surface when the Asp is indirectly connected to the rutile through a single outer-sphere mediating Mg^{2+} .

In case I (Ca^{2+}), the Ca^{2+}_{-2} ion in the position of the double outer-sphere mediating Mg^{2+}_{-2} in Figure 9a moves rapidly toward the rutile surface, adsorbing at a BD-TOTO site (Figure 12a-(1)). From the black curve in Figure 12a, it can be found that the single outer-sphere Ca^{2+}_{-1} converts into a BD-TOTO binding geometry and keeps bridging both O_{COO}^- atoms to the surface. The final Asp/rutile binding in case I (Figure 12a-(2)) is mediated by the BD-TOTO Ca^{2+}_{-1} (bound to both O_{COO}^-) and the BD-TOTO Ca^{2+}_{-2} (O_{CO} is H-bonded to the hydration waters of Ca^{2+}_{-1} and Ca^{2+}_{-2}). In case II (Ca^{2+}), the mediating Ca^{2+}_{-1} keeps indirectly connected to the rutile surface via the intermediate hydration waters during the entire simulation (Figure 12b, in a single outer-sphere mediation mode), assisting in maintaining the “horseshoe” configuration of RGD (Figure 12b-(1)). However, the $Ca^{2+}_{-1}-O_{COO}^-$ bond breaks, leaving only the O_{COO}^- atom coordinated to the mediating cation at $t = 3.7$ ns, when a water molecule approaches the Ca^{2+}_{-1} , penetrating into its first hydration shell (Figure 12b-(2)). Thus the loss of the direct bond between Ca^{2+}_{-1} and O_{COO}^- may

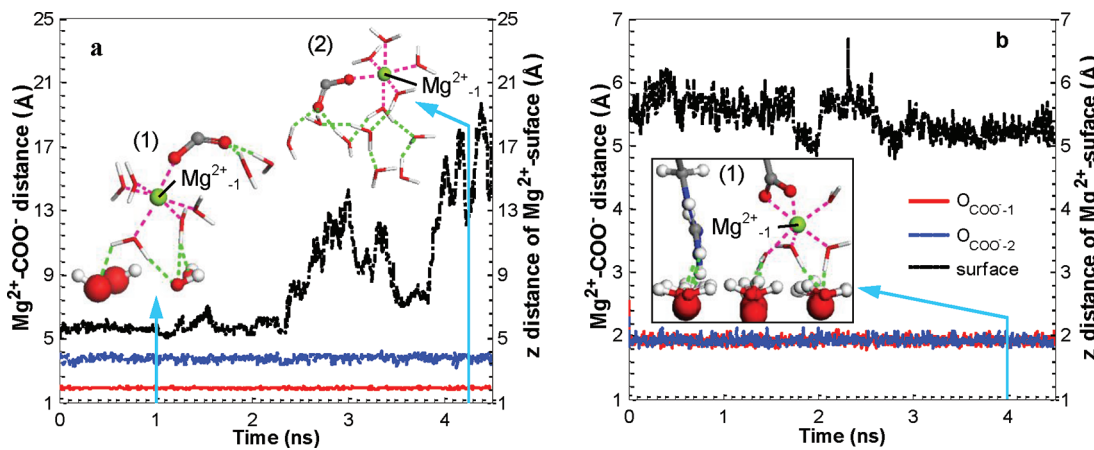


Figure 11. Evolution of the distances from the single outer-sphere mediating Mg^{2+-1} to the COO^- group, as well as the z position of this specific cation with respect to the rutile plane. (a) For case I (Mg^{2+}): placing the RGD+ Mg^{2+-1} complex (in Figure 9a) upward to allow the single outer-sphere mediation by Mg^{2+-1} , (b) for case II (Mg^{2+}): placing the RGD+ Ca^{2+-1} complex (in Figure 9b) upward to allow the single outer-sphere mediation by Ca^{2+-1} , and then replacing all the Ca^{2+} ions with the Mg^{2+} ions.

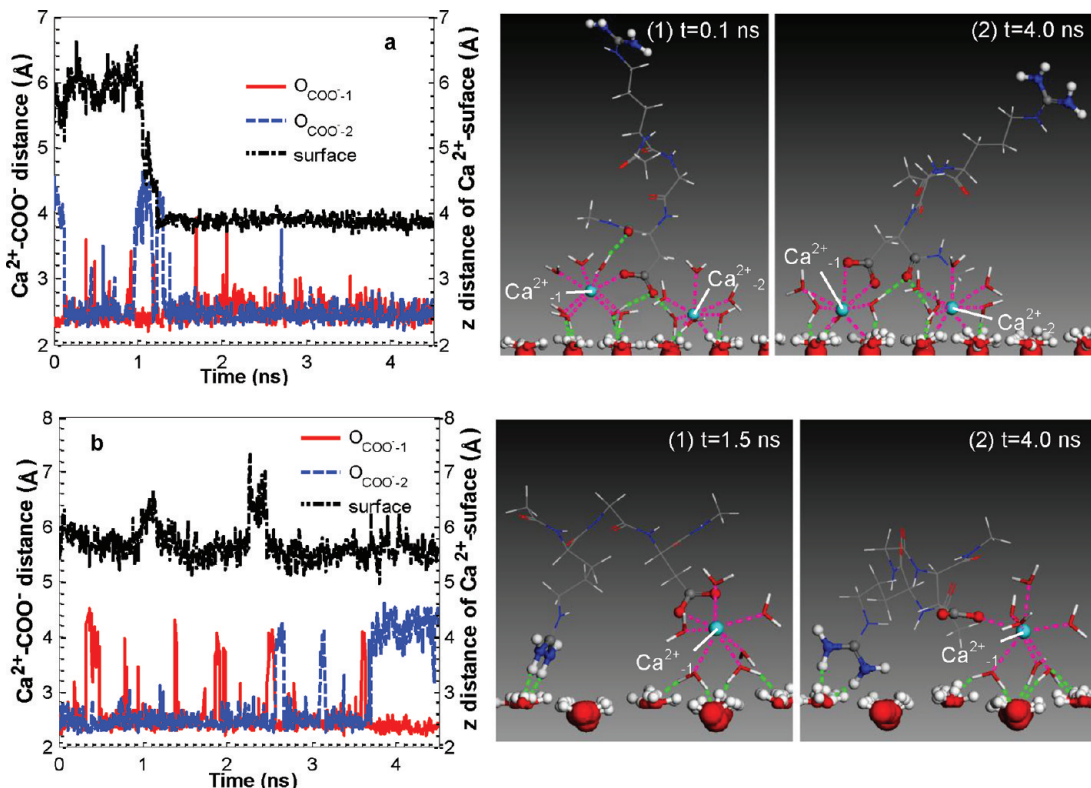


Figure 12. Evolution of the distances from the single outer-sphere mediating Ca^{2+-1} to the COO^- group, and the z -position of this specific cation with respect to the rutile plane, as well as the adsorption configurations at different time. (a) For case I (Ca^{2+}): placing the RGD+ Mg^{2+-1} complex (in Figure 9a) upward to allow the single outer-sphere mediation by Mg^{2+-1} , and then replacing all the Mg^{2+} ions with the Ca^{2+} ions, (b) for case II (Ca^{2+}): placing the RGD+ Ca^{2+-1} complex (in Figure 9b) upward to allow the single outer-sphere mediation by Ca^{2+-1} .

derive from the water competition, accompanied by the structural adjustment of the peptide for a favorable configuration.

Although the double outer-sphere mediation by Mg^{2+} lasts for a short time, the Mg^{2+} ion accompanied by its hydration shell is shown to be capable of bridging the peptide to the rutile surface through the COO^- ...water... Mg^{2+} ...water...rutile H-bond network. Moreover, the results outlined in this section further confirm that there seems to be a kinetic hindrance for outer-sphere to inner-sphere transition of the adsorbed Mg^{2+} .

When the Arg side chain of RGD moves freely in the solvent phase (not attached to the rutile surface, case I), the random diffusive motion will cause the entire peptide to slowly move away from the surface. The outer-sphere Mg^{2+-1} shows no tendency to further approach the surface, adsorbing at an inner-sphere site; thus the hydrogen bonds between the surface and the intermediate hydration waters of Mg^{2+-1} seem to be not strong enough to "trap" the $Mg^{2+-1}-O_{COO^-}$ complex on the surface, ending up with the departure of the Mg^{2+-1} -RGD complex. In contrast, the Ca^{2+-1} in the same case can move

from the outer-sphere region to the inner-sphere binding site on the present time scale, further strengthening the binding interaction between the mediating Ca^{2+} and the surface. These results arise from the “regular” lyotropic phenomenon, i.e., the smaller the cation, the larger the barrier to transition between the inner- and outer-sphere binding geometries, as a result of the greater cation–O (O_w or surface oxygens) attraction.

4. CONCLUSIONS

In the present study, we explored the molecular scale events that occur when RGD adsorbs to the negatively charged hydroxylated rutile (110) surface by employing classical MD simulations. The attention was focused particularly on the mediating role of the monovalent (Na^+ , K^+ , and Rb^+) and divalent (Mg^{2+} , Ca^{2+} , and Sr^{2+}) cations in Asp/rutile binding, where both of them are negatively charged. The simulation results indicate that the ionic radii and charges will significantly affect the hydration, binding mode and distance of the cation from the rutile surface. The monovalent cations with a loose hydration shell are more readily desolvated; thus their adsorption strength on the surface (characterized by the weighted average height of adsorbed cations from the rutile plane), in the order $\text{Na}^+ > \text{K}^+ > \text{Rb}^+$, shows a “reverse” lyotropic trend. In contrast, the adsorption strength of divalent cations, which are surrounded by a more tightly bound hydration shell, on the same surface increases with the increasing crystallographic radii ($\text{Sr}^{2+} > \text{Ca}^{2+} > \text{Mg}^{2+}$), exhibiting a “regular” lyotropic behavior.

The propensity of Asp/rutile binding is also demonstrated to be strongly influenced by the ionic properties. The TD geometry is the unique binding mode of monovalent cations in mediating the Asp/rutile interaction. In the NaCl, KCl, and RbCl solutions, the COO^- group remains H-bonded to the rutile surface during the entire simulation time, while the mediating monovalent cations can approach the Asp/rutile binding site to further stabilize the COO^- group on the surface. However, if the number of stable hydrogen bonds between the O_{COO}^- atoms and the H_{OH} atoms is large enough to “trap” the Asp side chain on the surface, the mediating cation is not essential to the Asp/rutile binding and free to leave. The divalent cations show a completely different mediation behavior. The strong attraction of the mediating divalent cations for the negatively charged Asp side chain causes the O_{COO}^- atoms to move farther away from the surface, thereby breaking the $\text{H}_{\text{OH}} \cdots \text{O}_{\text{COO}}^-$ hydrogen bonds. However, the link between the COO^- group and the surface provided by the mediating divalent cation is strong enough to “trap” the Asp side chain on the surface within the sampling time, even in the absence of H-bond connections between the COO^- group and the rutile surface. In addition to the inner-sphere mediation, single and double outer-sphere mediation modes of the divalent cations in peptide/rutile binding, which have not been reported previously,⁶⁰ are also found in the present simulations. However, there seems to be an energy barrier hindering the transition of the divalent cations between the inner- and outer-sphere mediation modes. The smaller the cation, the larger the barrier to transition, as a result of the greater cation–O (O_w or surface oxygens) attraction. If the outer-sphere mediating divalent cation cannot penetrate into the inner-sphere region (e.g., Mg^{2+}), it is possible that it will move away from the surface together with the peptide as a result of the random diffusive motion. This indicates that the barrier to transition is

the key to mediation of the peptide to the surface by divalent cations.

The present work has provided insights into the importance of cations in determining the binding propensities of peptides on the metal oxide materials. Divalent cations seem to be more effective and more stable than monovalent cations in bridging the negatively charged residue to the negatively charged surface, as reported in many experimental studies of cation mediation in adsorption of nucleic acids on the mineral surfaces.^{24–27} We anticipate that the findings presented will contribute to the understanding of the underlying mechanism of charge shielding and ion mediation on the charged surface at a molecular level, laying the groundwork for future research, which will ultimately allow specific manipulation of binding and assembly of proteins onto inorganic surfaces.

■ AUTHOR INFORMATION

Corresponding Author

*Tel: +86(0)451-86403252. Fax: +86(0)451-86403252. E-mail: wuchunya1982@163.com.

Present Address

[†]University of Dayton.

■ ACKNOWLEDGMENTS

This work was supported by the Research Fund for the Doctoral Program of Higher Education of China (No. 20102302110006). This research used resources of the National Energy Research Scientific Computing Center, which is supported by the Office of Science of the U.S. Department of Energy under Contract No. DE-AC02-05CH11231.

■ REFERENCES

- (1) Rammelta, S.; Illert, T.; Bierbaum, S.; Scharnweber, D.; Zwipp, H.; Schneiders, W. *Biomaterials* **2006**, *27*, 5561–5571.
- (2) Bauer, T. W.; Schils, J. *Skeletal Radiol.* **1999**, *28*, 423–432.
- (3) Moroni, A.; Heikkila, J.; Magyar, G.; Toksvig-Larsen, S.; Giannini, S. *Clin. Orthop.* **2001**, *388*, 209–217.
- (4) Sandén, B.; Olerud, C.; Petrén-Mallmin, M.; Larsson, S. *J. Bone Joint Surg. Br.* **2002**, *84-B*, 387–391.
- (5) Shepperd, J. A.; Aphorp, H. *J. Bone Joint. Surg. Br.* **2005**, *87*, 1046–1049.
- (6) Augat, P.; Claes, L.; Hanselmann, K. F.; Suger, G.; Fleischmann, W. *J. Appl. Biomater.* **1995**, *6*, 99–104.
- (7) Tisdel, C. L.; Goldberg, V. M.; Parr, J. A.; Bensusan, J. S.; Staikoff, L. S.; Stevenson, S. *J. Bone Joint Surg. Am.* **1994**, *76*, 159–171.
- (8) Ferris, D. M.; Moodie, G. D.; Dimond, P. M.; Gioranni, C. W. D.; Ehrlich, M. G.; Valentini, R. F. *Biomaterials* **1999**, *20*, 2323–2331.
- (9) Xiao, Y.; Truskey, G. A. *Biophys. J.* **1996**, *71*, 2869–2884.
- (10) Brighton, C. T.; Albelda, S. M. *J. Orthop. Res.* **1992**, *10*, 766–773.
- (11) Grzesik, W. J.; Robey, P. G. *J. Bone Miner. Res.* **1994**, *9*, 487–496.
- (12) Brandley, B. K.; Schnaar, R. L. *Anal. Biochem.* **1988**, *172*, 270–278.
- (13) Middleton, C. A.; Pendegrass, C. J.; Gordon, D.; Jacob, J.; Blunn, G. W. *J. Biomed. Mater. Res., Part A* **2007**, *83*, 1032–1038.
- (14) Dee, K. C.; Puleo, D. A.; Bizios, R. *An Introduction to Tissue-Biomaterial Interactions*; John Wiley & Sons: New York, 2003.
- (15) Skelton, A. A.; Liang, T.; Walsh, T. R. *ACS Appl. Mater. Interfaces* **2009**, *1*, 1482–1491.
- (16) Kang, Y.; Li, X.; Tu, Y. Q.; Wang, Q.; Ågren, H. *J. Phys. Chem. C* **2010**, *114*, 14496–14502.

- (17) Horinek, D.; Serr, A.; Geisler, M.; Pirzer, T.; Slotta, U.; Lud, S. Q.; Garrido, J. A.; Scheibel, T.; Hugel, T.; Netz, R. R. *Proc. Natl. Acad. Sci. U.S.A.* **2008**, *105*, 2842–2847.
- (18) Forte, G.; Grassi, A.; Marletta, G. *J. Phys. Chem. B* **2007**, *111*, 11237–11243.
- (19) Chen, M. J.; Wu, C. Y.; Song, D. P.; Li, K. *Phys. Chem. Chem. Phys.* **2010**, *12*, 406–415.
- (20) Lüthen, F.; Lange, R.; Becker, P.; Rychly, J.; Beck, U.; Nebe, J. G. B. *Biomaterials* **2005**, *26*, 2423–2440.
- (21) Yin, G.; Liu, Z.; Zhan, J.; Ding, F. X.; Yuan, N. J. *Chem. Eng. J.* **2002**, *87*, 181–186.
- (22) Wu, C. Y.; Skelton, A. A.; Chen, M. J.; Vlček, L.; Cummings, P. T. *J. Phys. Chem. C* **2011**, *115*, 22375–22386.
- (23) Thomson, N. H.; Kasas, S.; Smith, B.; Hansma, H. G.; Hansma, P. K. *Langmuir* **1996**, *12*, 5905–5908.
- (24) Poly, F.; Chenu, C.; Simonet, P.; Rouiller, J.; Monrozier, L. J. *Langmuir* **2000**, *16*, 1233–1238.
- (25) Libera, J. A.; Cheng, H.; Olvera de la Cruz, M.; Bedzyk, M. J. *J. Phys. Chem. B* **2005**, *109*, 23001–23007.
- (26) Cheng, H.; Zhang, K.; Libera, J. A.; Olvera de la Cruz, M.; Bedzyk, M. J. *Biophys. J.* **2006**, *90*, 1164–1174.
- (27) Romanowski, G.; Lorenz, M. G.; Wackernagel, W. *Appl. Environ. Microbiol.* **1991**, *57*, 1057–1061.
- (28) Dumont, F.; Warlus, J.; Watillon, A. *J. Colloid Interface Sci.* **1990**, *138*, 543–554.
- (29) Bérubé, Y. G.; de Bruyn, P. L. *J. Colloid Interface Sci.* **1968**, *28*, 92–105.
- (30) Čolić, M.; Fuerstenau, D. W.; Kallay, N.; Matijević, E. *Colloids Surf., A* **1991**, *59*, 169–185.
- (31) Kallay, N.; Čolić, M.; Fuerstenau, D. W.; Jang, H. M.; Matijević, E. *Colloid Polym. Sci.* **1994**, *272*, 554–561.
- (32) Lyklema, J.; Overbeek, J.; Th., G. *J. Colloid Sci.* **1961**, *16*, 595–608.
- (33) Grahame, D. C. *J. Am. Chem. Soc.* **1941**, *63*, 1207–1215.
- (34) Bourikas, K.; Hiemstra, T.; van Riemsdijk, W. H. *Langmuir* **2001**, *17*, 749–756.
- (35) Dumont, F.; Watillon, A. *Discuss. Faraday Soc.* **1971**, *52*, 352–360.
- (36) Breeuwsma, A.; Lyklema, J. *Discuss. Faraday Soc.* **1971**, *52*, 324–333.
- (37) Sprycha, R. *J. Colloid Interface Sci.* **1989**, *127*, 1–11.
- (38) Lyklema, J. *Adv. Colloid Interface Sci.* **2003**, *100–102*, 1–12.
- (39) Ridley, M. K.; Machesky, M. L.; Palmer, D. A.; Wesolowski, D. *Colloids Surf., A* **2002**, *204*, 295–308.
- (40) Předota, M.; Vlček, L. *J. Phys. Chem. B* **2007**, *111*, 1245–1247.
- (41) Sano, K. I.; Shiba, K. *J. Am. Chem. Soc.* **2003**, *125*, 14234–14235.
- (42) Marcus, Y. *Chem. Rev.* **1988**, *88*, 1475–1498.
- (43) Gavryushov, S. *J. Phys. Chem. B* **2009**, *113*, 2160–2169.
- (44) Předota, M.; Zhang, Z.; Fenter, P.; Wesolowski, D. J.; Cummings, P. T. *J. Phys. Chem. B* **2004**, *108*, 12061–12072.
- (45) Dang, L. X. *J. Am. Chem. Soc.* **1995**, *117*, 6954–6960.
- (46) LAMMPS Molecular Dynamics Simulator Home Page. <http://lammps.sandia.gov> (accessed Jan 18, 2011).
- (47) Cornell, W. D.; Cieplak, P.; Bayly, C. I.; Gould, I. R.; Merz, K. M. Jr; Ferguson, D. M.; Spellmeyer, D. C.; Fox, T.; Caldwell, J. W.; Kollman, P. A. *J. Am. Chem. Soc.* **1995**, *117*, 5179–5197.
- (48) Bandura, A. V.; Kubicki, J. *J. Phys. Chem. B* **2003**, *107*, 11072–11081.
- (49) Předota, M.; Bandura, A. V.; Cummings, P. T.; Kubicki, J. D.; Wesolowski, D. J.; Chialvo, A. A.; Machesky, M. L. *J. Phys. Chem. B* **2004**, *108*, 12049–12060.
- (50) Hoover, W. G. *Phys. Rev. A* **1985**, *31*, 1695–1697.
- (51) Ryckaert, J. P.; Ciccotti, G.; Berendsen, H. J. C. *J. Comput. Phys.* **1977**, *23*, 327–341.
- (52) Vahvaselkä, K. S.; Mangs, J. M. *Phys. Scr.* **1988**, *38*, 737–741.
- (53) Impey, R. W.; Madden, P. A.; McDonald, I. R. *J. Phys. Chem.* **1983**, *87*, 5071–5083.
- (54) Marcus, Y. *Ion Properties*; Marcel Dekker, Inc: New York, 1997.
- (55) Caminiti, R.; Licheri, G.; Piccaluga, G.; Pinna, G. *J. Appl. Crystallogr.* **1979**, *12*, 34–38.
- (56) Albright, J. N. *J. Chem. Phys.* **1972**, *56*, 3783–3786.
- (57) Caminiti, R.; Licheri, G.; Paschina, G.; Piccaluga, G.; Pinna, G. *J. Chem. Phys.* **1980**, *72*, 4522–4528.
- (58) Palinkas, G.; Radnai, T.; Hajdu, F. Z. Z. *Naturforsch., Teil A* **1980**, *35*, 107–114.
- (59) Ohtomo, N.; Arakawa, K. *Bull. Chem. Soc. Jpn.* **1980**, *53*, 1789–1794.
- (60) Monti, S.; Alderighi, M.; Duce, C.; Solaro, R.; Tiné, M. R. *J. Phys. Chem. C* **2009**, *113*, 2433–2442.